Enhanced Neurite Outgrowth and Regeneration in ALS Resistant Motor Neurons from SOD1 Mutant Mouse Models

Zachary Osking[1], Jacob I. Ayers[2,3,4], Ryan Hildebrandt[5], Kristen Skruber[1], Hilda Brown[2,3], Daniel Ryu[2,3], Amanda R. Eukovich[1], Todd E. Golde[2,3,4], David R. Borchelt[2,3,4], Tracy-Ann Read[1*] and Eric A. Vitriol[1*]

[1]Department of Anatomy and Cell Biology, [2]Department of Neuroscience, [3]Center for Translational Research in Neurodegenerative Disease, [4]McKnight Brain Institute, and [5]Department of Molecular Genetics and Microbiology, University of Florida, Gainesville, FL, USA, 32610

*To whom correspondence should be addressed: Tracy-Ann Read, taread@ufl.edu; Eric Vitriol, evitriol@ufl.edu

Abstract

Amyotrophic lateral sclerosis (ALS) is a progressive and fatal neurodegenerative disease characterized by motor neuron cell death and subsequent paralysis of voluntary muscles. Although ALS specifically affects motor neurons, some cells are resistant to disease progression. Most ALS studies have focused on the cellular mechanisms that cause loss of motor neuron viability. Less is known about the surviving neurons, and most of that information has come from gene expression profiling. In this study, we functionally characterize the surviving spinal motor neurons by culturing them from SOD1 ALS mouse models at various stages of disease progression. Surprisingly, we found that in comparison to non-transgenic controls, ALS resistant motor neurons from adult $SOD1^{G93A}$ mice have enhanced axonal outgrowth and dendritic branching. Further, the enhanced outgrowth occurs before the mice become symptomatic, but increases with disease progression. Motor neurons from $SOD1^{G93A}$ mice also display an increase in the number and size of actin-based structures such as growth cones and filopodia. The increased outgrowth and branching phenotype is predominantly cell-intrinsic and can be induced in motor neurons from non-transgenic mice by exogenous expression of $SOD1^{G93A}$. These results indicate that expression of mutant SOD1 in ALS-resistant adult motor neurons can enhance their regenerative capability via a mechanism that is not directly correlated with the onset of ALS symptoms. Understanding the positive effects that mutant SOD1 has on motor neuron regeneration could lead to new therapeutic strategies that capitalize on this mechanism.

Keywords

Amyotrophic lateral sclerosis; SOD1, motor neuron, growth cone, actin, cytoskeleton

Abbreviations

ALS	Amyotrophic lateral sclerosis
MN	motor neuron
SOD1	superoxide dismutase 1
GFP	green fluorescent protein
YFP	yellow fluorescent protein
NTg	non-transgenic
G93A	transgenic mouse line expressing SOD1 with a glycine-to-alanine mutation at position 93
G93A-DL	transgenic mouse line expressing SOD1 with a glycine-to-alanine mutation at position 93 with a lower copy number than the G93A mouse line
G85R	transgenic mouse line expressing SOD1 with a glycine-to-arginine mutation at position 85 fused to YFP

Introduction

Amyotrophic lateral sclerosis (ALS) is a fatal, adult-onset neurodegenerative disorder in which there is selective loss of motor neurons (MNs) in the cerebral cortex, brainstem and spinal cord [35]. Not all MNs are equally susceptible to cell death during ALS disease progression. ALS mostly targets MNs required for voluntary movement, whereas MNs of the autonomic system are less affected [57]. Certain groups of somatic motor neurons, including those in the oculomotor nucleus and Onuf's nucleus, are also generally spared [25, 32, 51, 69]. Furthermore, there is a gradient of vulnerability among spinal MNs, where faster motor units become affected before slower muscle types [58]. MNs that are less ALS-susceptible can compensate for the cells that initially die by establishing new connections with the motor endplate, although many of these will eventually succumb to the disease [64].This selective neuronal vulnerability is present in both sporadic ALS and familial ALS and is also recapitulated in rodent models, such as the SOD1^{G93A} mouse [51]. The mechanism that renders certain subgroups of MNs more susceptible to ALS is largely unknown, although studies have shown that ALS resistant MNs differentially express GABA and glutamate receptor subunits [45], [44], [13] and show a higher expression of EGR1, IGF2 [3] and OPN [48]. On the other hand, ALS vulnerable MNs have high expression of matrix metalloproteinase-9 (MMP9) [11] which was identified as a modulator of ER stress [37, 39], supporting previous studies showing that such ALS vulnerable MNs are selectively prone to ER stress [63].

Approximately 90% of ALS cases are sporadic with unknown etiology; the remaining 10% are inherited and known as familial ALS (fALS), of which over 20% have mutations in the gene encoding Cu/Zn superoxide dismutase 1 (SOD1) [14]. To date, over 155 different mutations have been identified in SOD1 either in isolated cases of ALS or more commonly in patients from families showing autosomal dominant patterns of inheritance [4, 55]. ALS-linked SOD1 mutations are thought to induce a toxic gain-of-property of the protein, which becomes prone to misfolding and subsequent aggregation [38, 61]. While the exact cause of SOD1-induced MN degeneration is unknown, a number of pathogenic processes, including excitotoxicity, oxidative stress, mitochondrial dysfunction, dysregulation of the cytoskeleton, axonal transport defects, and inflammation are considered to play important roles in eventually inducing cell death [22, 34]. Some of the most significant advances in our understanding of how mutations in the SOD1 gene cause ALS have been achieved through rodent models. Since the generation of the first SOD1^{G93A} transgenic mouse line [31], several other mutant SOD1 models now exist with slight variation in their pathologies, including time to onset of symptoms and death [15, 36, 50]. The SOD1^{G93A} mouse (referred to here as G93A) carries 22 copies of a causative mutation (a glycine-to-alanine replacement at residue 93) in the human SOD1 gene, inserted randomly into chromosome 12 of the mouse genome [2]. This mouse model has an onset of paralysis at ~90 days, accompanied by degenerative motor neuron loss similar to that of human ALS pathology [66], and death by 130-180 days depending on the genetic background and gender of the mice. The G93A mouse remains the most widely used model of human ALS [31] to date.

While most studies have focused on the cellular mechanisms and genes that induce MN death in ALS, less is known about the neurons that do survive, including their ability to resist stress-induced

cell death and to compensate for dying MNs. Most of our current knowledge about surviving spinal MNs in ALS mouse models has largely been generated by gene expression profiling of both whole spine and micro-dissected tissue and cells [6, 13, 20, 21, 41, 63]. However, these studies provide just a single snapshot of the MN's biology and only allow for inferences to be made about how changes in gene expression alter MN physiology, allow them to resist degeneration, or compensate for dying neurons by forming new motor endplate attachments. In the current study, we sought to functionally characterize ALS-resistant MNs by culturing them *in vitro*, where we would be able to directly assess dynamic cellular properties such as outgrowth, branching, and regulation of the cytoskeleton. We found that in comparison to age-matched, non-transgenic controls, ALS-resistant motor neurons cultured from G93A mouse models have enhanced axonal outgrowth and dendritic outgrowth/branching. They also have an increase in both number and size of actin-based cell structures such as growth cones and filopodia. Interestingly, enhanced outgrowth and branching occurs in pre-symptomatic mice but increases with the onset of ALS symptoms. This phenotype occurs independently of SOD1 enzymatic activity and can only slightly be enhanced by non-cell autonomous factors. Exogenous expression of mutant SOD1 in non-transgenic adult motor neurons is sufficient to induce the enhanced outgrowth phenotype. These results indicate that expression of mutant SOD1 in adult motor neurons can enhance their regenerative capability via a cell intrinsic mechanism that is not directly correlated with ALS onset. Identifying the signaling pathways and functional mechanisms involved in this regenerative response could open up novel avenues for experimental treatments for ALS patients.

Materials and Methods

Mouse colony housing and breeding

All studies involving mice were approved by the Institutional Animal Care and Use Committee (IACUC) at the University of Florida in accordance with NIH guidelines. Adult mice were housed one to five per cage and maintained on *ad libitum* food and water, with a 12 h light/dark cycle. Transgenic mouse strains SOD1-G93A and SOD1-G93A-DL (JAX stock #004435 and #002299 respectively [31] were purchased from Jackson laboratory (Bar Harbor, Maine), and bred by the Rodent Breeding Services offered by the Animal Care Services at the University of Florida. SOD1-G93A and SOD1-G93-DL colonies were maintained by breeding hemizygous mice either to wild type siblings, or to C57BL/6J inbred mice (Jax Stock # 000664). Additional transgenic mice strains used in this study were G85R-SOD1:YFP [74] and WT-SOD1 (JAX stock #002297), both strains were generously supplied by Dr. Borchelt. The G85R-SOD1:YFP mice were maintained as heterozygotes on the FVB/NJ background and whereas the WT-SOD1 were maintained on a C57Bl/6J and C3H/HeJ hybrid background. For the studies involving G85R-SOD1:YFP mice which were induced to develop ALS, please refer to a full description of the procedure by Ayers *et al* [5].In addition to the adult mice, we also used timed-pregnant C57BL/6J and SOD1-G93A-DL mice at gestational day 14, which were also generated by the Rodent Breeding Services offered by the Animal Care Services at the University of Florida.

Colony maintenance genotyping for all strains was performed as previously described [31, 73]. Furthermore, to control for possible transgene copy loss due to meiotic rearrangement, breeders were regularly screened by RT-PCR as previously described [33] and replaced with fresh founder stocks from Jackson laboratory (Bar Harbor, Maine) every 5 generations. In our colony SOD1-G93A and SOD1-G93-DL mice reached late disease stage at 150-180 days and 240-330 days of age respectively.

Assessment of ALS disease progression

Mice were considered symptomatic if they displayed a 15% loss of bodyweight or showed signs of leg paralysis, whichever was reached first. In our hands, the majority of mice (~70%) were euthanized because of leg paralysis, and the rest due to decreased body weight. All mice were euthanized by CO_2 inhalation following the guidelines provided by the University of Florida Animal Care Services (ACS) and approved by the Institutional Animal Care and Use Committee (IACUC).

Study design

To control for gender differences in disease progression and phenotype of SOD1-G93A mice, symptomatic adult G93A and G93A-DL mice were always paired with non-transgenic (NTg) mice of the same gender and of similar age for each experiment, in most cases using littermates. Age and gender matching also allowed us to control for batch differences in the conditioned medium used to culture adult MN as described below under “cell culture conditions”.

Adult and embryonic mouse spinal cord isolation

Embryo spinal cords were obtained from timed pregnant G93A-DL and C57BL/6J mice at embryonic day 14 as previously described in detail [7]. Once embryos were removed from the uterus, spinal cords were extracted under sterile conditions in a laminar flow hood with the aid of a dissecting microscope (SMZ800, NIKON INSTRUMENTS INC.) and small forceps and placed into cold Leibovitz's L-15 medium (Life Technologies, Grand Island, NY) supplemented with 25 µg ml^{-1} penicillin-streptomycin (Life Technologies). The meninges and dorsal root ganglia (DRG) were peeled off and individual spinal cords were transferred into a 12 wells plate, identified and kept in cold L-15 medium on ice. Tails from each embryo were also harvested at this point for genotyping (G93A-DL mice).

Adult spinal cords were isolated by cutting the vertebrate column with scissors in front of the back legs and just below the medulla oblongata and flushed out of the spinal column using a syringe filled with cold supplemented DMEM/F12-medium with 18G needle (BD Biosciences). The DMEM/F12-medium used for this purpose consisted of DMEM/F12 in a 3:1 ratio supplemented with 36.54 mM NaHCO3 (Fisher Scientific), 0.18 mM L-adenine (Sigma), 312.5 µl L^{-1} 2N HCL (Fisher Scientific), 10% of fetal calf serum (Hyclone, GE Healthcare Life Sciences, South Logan, Utah) and 25 µg ml^{-1} of penicillin-streptomycin (Life Technologies). The adult spinal cords were transferred into cold DMEM/F12-medium.

MN cell extraction and separation

Both embryonic and adult motor neurons were extracted using the method and reagents described in detail by Beaudet *et al*. [7] with a few modifications. Briefly, individual spinal cords were cut into small pieces and incubated for 30 min at 37°C in digestion buffer consisting of Dulbecco's PBS (DPBS, Life Technologies, Grand Island, NY) containing 10 U/ml^{-1} papain (Worthington, Lakewood, NJ, USA), 200 $\mu g/ml^{-1}$ L-cysteine (Sigma St. Louis, MO) and 250 U/ml^{-1} DNase (Sigma, St. Louis, MO). The digestion buffer was then removed and replaced with DPBS containing 8 mg/ml Ovomucoid trypsin inhibitor (Sigma), 8 mg/ml bovine serum albumin (BSA, Sigma), and 250 U/ml DNase. The tissue was then triturated using glass pipettes to obtain a single-cell suspension This step was repeated trice before all cells were collected and filtered through a 40 µm cell strainer (BD Falcon) and centrifuged at 280 g for 10 min at 4 °C for MN. Adult mixed motor neuron cultures were ready to plate after this step. Embryonic MN pellets were enriched by resuspending in 6 ml of cold Leibovitz's L-15 medium (Life Technologies) and laid over a 1.06 g ml−1 Nycoprep density solution (Axis-Shield, Dundee, Scotland) and spun at 900 g for 20 min at 4 °C without brake in a swinging bucket centrifuge (Eppendorf, Hauppauge, NY). MN were collected at the interface of the Nycoprep solution and poured in a new 50 ml collection tube which was then filled with cold L-15. MN cells were counted at this step. MN collecting tubes were centrifuged at 425 g for 10 min in a swinging bucket centrifuge at 4°C.

Cell culture

Embryonic MN pellets were gently resuspended at 200,000 cells/cm^2 in freshly prepared Motor Neuron Growth Medium (MNGM), which is described in detail by Graber DJ *et al* [27]. Briefly, the MNGM consists of Neurobasal A medium (NB-medium, Life Technologies) supplemented with 1X B-27 Serum-Free Supplement (Gibco/Life Technologies), 1X SATO supplement, 5 µg mL^{-1} Insulin

(Gibco/Life Technologies), 1 mM Sodium pyruvate (Gibco/Life Technologies), 2 mM L-Glutamine (Gibco/Life Technologies), 40 ng mL^{-1} of 3,3,5-triiodo-L-thyronine sodium salt (T3; Sigma-Aldrich), 1 µg mL^{-1} Mouse laminin (Gibco/Life Technologies), 417 ng mL^{-1} Forskolin (Sigma-Aldrich), 5 µg mL^{-1} N-acetyl-L-cysteine (NAC, Sigma-Aldrich) and 1x Penicillin-streptomycin (Gibco/Life Technologies). After filter-sterilization using a 22 µm syringe filter, 10 ng mL^{-1} of each of the following growth factors was added to the medium: brain-derived neurotrophic factor (BDNF; Sigma-Aldrich), ciliary neurotrophic factor (CNTF; Peprotech, Rocky Hill, NJ) and glial-derived neurotrophic factor (GDNF; Peprotech). Embryonic MNs were either seeded on to Poly-D-lysine (PDL) coated 6cm tissue culture plates (10 µg mL^{-1} PDL, Sigma-Aldrich) to generate conditioned medium used for adult MN cultures, or on to 1.5 cm glass coverslips pre-coated first with PDL (10 µg mL^{-1} for 1h at RT) then with Human Placental Laminin for 3 h at 37°C (1.67 µg mL^{-1} laminin in NB-Medium, Sigma-Aldrich). Embryonic motor neurons grown on coverslips were cultured for 3 days prior to fixation in 4% PFA and immunostaining for imaging and growth analysis.

Adult mixed motor neuron cultures were seeded onto PDL coated cover slips (10 µg $mL^{-1)}$ and cultured in MNGM which had been pre-conditioned for 4 days by embryonic motor neurons isolated from NTg C57BL/6J mice. Given that adult MN pallets contain considerable amount of debris when first plated, cells were not counted prior to seeding. After the cells were allowed to attach to the coverslips in a humidified 37°C incubator for 1 h, they were washed twice with warm NB-medium to remove debris and cultured in 1 ml of conditioned MNGM mixed 1:1 with freshly prepared MNGM. Adult MNs were cultured for 2 days prior to fixation and immunostaining for imaging and growth analysis. MN's where selected for analysis based on their expression of Tuj1, their large size, multi-polarity, and stellate cell shape.

Immunofluorescence

Cells were fixed with 4% electron microscopy grade paraformaldehyde (PFA, Electron Microscopy Sciences, Hatfield, PA) for 10 min at RT, permeabilized with 0.2% Triton X-100 (Sigma-Aldrich) for 3 min, and washed twice with 1X DPBS. Cells were stained overnight at 4°C with primary antibodies diluted in immunofluorescence staining buffer. They were then washed twice with DPBS for 5 min, incubated with secondary antibodies (diluted 1:1000) for 1 hr at room temperature in immunofluorescence staining buffer. F-actin was stained with Phalloidin-568 (diluted 1:100, Life Technologies) for 30 min at room temperature in immunofluorescence staining buffer. Finally, cells were washed three times with DPBS before mounting with Prolong Diamond W/ DAPI (Life Technologies). We used the following antibodies/stains: Mouse anti- β3 Tubulin (TUJ1 1:500 dilution, Covance, Princeton, NJ), Goat anti-ChAT (1:1000, AB144, ED Millipore), Mouse anti-Tau (1:25000, gifted from the Giasson lab [65]) Alexa Fluor™ Phalloidin 568, anti-mouse IgG 488 and anti-rabbit IgG 488 (Life Technologies) used at 1:1000.

Imaging

Imaging of IF stained motor neurons was performed on a Nikon A1R+ laser scanning confocal microscope with 40X 1.3 NA and 60X 1.49 NA objectives and the GaAsP multi-detector unit. Imaging

of cells for outgrowth and branching pattern analysis was done using the EVOS XL digital inverted microscope (Life Technologies).

Image analysis

Neurite growth cone analysis: Confocal z-stacks were converted into a single maximum intensity projection image. Terminal neurite growth cone size, filopodia length, and filopodia number were analyzed using Fiji (ImageJ) software. Filopodia length was defined as the distance between lamellipodium edge to the furthest end of the extending filopodia. Values were exported into Microsoft Excel and Graphpad Prism for statistical analysis.

Neurite tracing and branching analysis: Images were taken on the EVOS XL digital inverted microscope and imported into Fiji (ImageJ) software. All visible projections in these images were traced using the Simple Neurite Tracer plugin [43]. An image stack was created from the tracing which was then analyzed using the Sholl analysis plugin [23]. To compare the relative change in neuron radius between NTg and SOD1 mutants across different experiments each set was normalized to the average radius of the age matched NTg control group. The Sholl profile containing the number of branches per given distance from soma and overall neuron radius was then exported to Microsoft Excel or Graphpad Prism for analysis.

Axon tracing and analysis

Staining of motor neuron cultures were performed as previously described with a mouse-anti Tau antibody. Imaging was performed on the EVOS XL digital inverted microscope and the images were imported into Fiji (ImageJ) software. The 16-bit color lookup table was applied to each image to visualize the intensity of Tau-staining in the neurites. The neurite that was most intensely stained for Tau was then measured from the center of the soma to determine if it was the longest projection from the cell.

Adeno-associated virus (AAV) mediated overexpression of mutant SOD1 in adult MNs

MNs from adult (9-12 months) NTg mice were isolated and plated as described above. On the day they were plated, 20 µl of AAV2/8 (titer $1X10^9$) expressing WT SOD1-YFP, G93A SOD1-YFP and GFP only was added to the wells and the cells were cultured for 10 days (growth medium was refreshed every 5 days). For these experiments we used a self-complementary virus (scAAV), driven by the chick beta actin promotor (CBA) as described in [60]. After 10 days in culture, cells were fixed, stained for Tuj1 and imaged/analyzed as described below.

Results and Discussion

ALS-resistant G93A motor neurons have enhanced neurite outgrowth

Using a well characterized protocol for adult motor neuron extraction [7], we isolated MNs from whole spinal cords from SOD1^{G93A} high copy number mice (referred to as G93A) at late disease stage (defined by hind leg paralysis/weight loss), occurring between postnatal days 150 and 180. Cells were cultured for two days *in vitro* and immunostained for β3 tubulin (Tuj1) and Choline Acetyltransferase (ChAT) to confirm our success in isolating MNs (Supplemental Fig. 1) as described by others [7]. For imaging and analysis purposes, we stained the cells with Tuj1 and phalloidin (for actin visualization) and selected MNs based on their large soma size, multi-polarity and Tuj1 positive staining. Importantly, MN cultures from ALS mouse models were always made in parallel with MN cultures from sex- and age-matched, non-transgenic littermates (NTg) to control for experimental variability. During cell isolation, all established neuronal projections are severed, thus this assay is a direct measurement of the cells' ability to generate new processes. We performed a large-scale quantitative analysis of MN size and branching complexity by tracing the neurons and performing Sholl analysis. Interestingly, MNs from G93A mice displayed substantially increased outgrowth in comparison to NTg MNs, both in neurite length (~40% longer than NTg cells) and number of branches per cell (Fig. 1a-d). While it is known that ALS-resistant MNs have altered RNA expression profiles, including some genes involved in cytoskeletal pathways, the genetic changes observed are usually associated with the negative regulation of outgrowth [56]. Hence, we were surprised to discover that ALS-resistant MNs actually have an enhanced capacity for outgrowth following neurite severing.

While the G93A mouse is the most extensively studied rodent model of ALS, there is some concern about its use given that such a high copy number of the transgene is required to generate the rapid onset of ALS symptoms. This is in contrast to human SOD1-based ALS, where individuals expressing 1 copy of mutant SOD1 at endogenous levels can develop the disease. To determine if the enhanced outgrowth of G93A MNs could occur with a more physiologically relevant level of expression, we cultured cells from another mouse model, SOD1^{G93A}-DL (referred to as G93A-DL), which only has 6-8 transgene copies per cell, hence referred to as dilute (DL) [1]. These mice still get ALS, but disease progression is slower, with a delayed end-stage occurring when the mice are between 8-11 months of age. Surprisingly, MNs isolated from end-stage G93A-DL mice exhibited an even greater outgrowth capacity over age-matched NTg MNs than that observed for the G93A MNs. Compared to controls, G93A-DL exhibit a ~55% median outgrowth length increase (Fig.1f, g) and had more than twice the number of branches >40 μm away from the cell body (Fig. 1f, h), with a continuous increase to more than 3 times as many branches at 70μm away from the cell body (Fig.1f). Thus, the enhanced outgrowth phenotype was still present in motor neurons from a G93A mouse with more moderate overexpression of the transgene.

To determine if the increased outgrowth of neurites also meant an increase in axonal regeneration, we stained the cells with anti-Tau to distinguish axons from dendrites. Based on having the highest Tau fluorescence intensity, we determined that 63% of the cells analyzed had a process that could be identified as the axon. Of these cells, the neurite with the highest Tau fluorescence was also the

longest process 79% of the time (Supplemental Fig. 2). This implies that, in addition to the observed increase in dendritic arborization as defined by the number of processes, the enhanced increase in overall cell radius (reported as length) corresponds to enhanced axonal regeneration.

The G93A mutation preserves the enzymatic activity of SOD1, which is to remove superoxide radicals. Reactive oxygen species (ROS) such as superoxide ($O_2^{\bullet-}$), hydrogen peroxide (H_2O_2) and the hydroxyl radical (OH^-) are used by neurons in intracellular signaling events during apoptosis, differentiation, and cell migration [46, 68]. Hence, a potential explanation for the enhanced outgrowth seen in ALS-resistant MNs from G93A and G93A-DL mice might be that the neurons have altered redox signaling that promotes neurite extension. To test for this, we cultured MNs from heterozygote mice overexpressing wild-type human SOD1 (referred to as WT-SOD1). Additionally, WT-SOD1 mice do not get ALS [24, 29], which reduces the possibility of an activated MN stress response. Relative to age-matched NTg control MNs, WT-SOD1 MNs actually exhibited a slight decrease in outgrowth and branching (Fig. 1i-l). This is consistent with previous findings where ROS depletion in neurons has been shown to have negative effects on neurite outgrowth [49]. Therefore, it is unlikely that the enhanced outgrowth of G93A MNs is attributed to increasing the level of enzymatically active SOD1.

Another potential explanation for the enhanced outgrowth phenomenon we observed is that ALS-resistant G93A cells grow bigger because they are actually larger cells to begin with. This notion is contradictory to published *in vivo* studies of spinal cord tissue from patients and mouse models with ALS, where surviving MNs have significantly reduced soma size due to the small γ fusimotor neurons (γ-MNs) being selectively disease resistant [40]. However, since no previous studies have characterized the size of cultured ALS-resistant MNs from adult mice, we sought to determine if the cells that generate the longest neurites were also the largest cells. We measured the soma of NTg, G93A, and G93A-DL MNs to determine if neurite growth correlated with the size of the cell body. While the mean soma area did increase significantly in G93A and G93A-DL MNs compared to NTg cells, we found that within each group, soma area was not correlated with neurite length and could therefore not be used to predict outgrowth (Supplemental Fig. 3). Thus, cell size is not a potential explanation for the increased outgrowth and branching phenotype seen in G93A and G93A-DL MNs.

Mutant SOD1 MNs acquire enhanced ability to regenerate before onset of ALS symptoms

Having established that end-stage ALS-resistant MNs from both G93A and G93A-DL mouse models have an enhanced capacity for neurite outgrowth and branching, we next wanted to determine if this was a survival response to ALS-induced cell death or if the neurons acquired this phenotype before the onset of symptoms. To do so, we first cultured MNs from presymptomatic G93A-DL mice at one, two and six months of age, and measured the outgrowth and branching. We found that G93A-DL MNs from one month old mice had identical outgrowth compared to NTg cells, and then began to grow significantly larger beginning at two months of age. This trend continues as the mice age and grow closer to the onset of ALS symptoms at 9 months old (Fig. 2a, b). In comparison, MNs from 2-month-old G93A mice did not display any enhanced outgrowth capacity (Fig. 2c-e). It is interesting that a pre-symptomatic phenotype was only seen in cells expressing low levels of G93A, though perhaps this may reflect a difference in how the disease develops between the two mouse models: sudden onset

with rapid progression for the G93A mouse and slower, more gradual progression of symptoms for the G93A-DL mouse. Alternatively, this might reflect that there is an age-dependent outgrowth response of this neuronal sub-population in the presence of $SOD1^{G93A}$, and that the G93A mice die before their suriving motor neurons are old enough to have the strongest regenerative potential.

To further confirm that the enhanced outgrowth of ALS-resistant MNs is not triggered by disease onset, we cultured cells from heterozygous mice overexpressing $SOD1^{G85R}$ fused with yellow fluorescent protein (YFP) (referred to as G85R mice). G85R is another well-documented mutant of SOD1 where mice homozygote for the transgene develop ALS, whereas heterozygotes never develop symptoms [72]. Hence, this is a useful model for studying the effects of the mutation at low dosage in the absence of disease onset. Surprisingly we found that G85R MNs cultured from 6-month-old mice displayed a similar increase in branching and outgrowth as MNs from G93A mouse models, although the branching pattern was somewhat different, with the most significant differences (double the number of branches) occurring between 50-80 µm from the soma (Fig. 2f-h). Given that the heterozygote G85R mice do not develop ALS, the motor neurons extracted from these mice have not been subjected to selection through disease resistance and thus represent all adult MNs with SOD1 mutations, not just those resistant to ALS. Thus, the enhanced outgrowth phenotype is not directly caused by the onset of ALS. To determine if this inherent outgrowth phenotype would be further enhanced with ALS disease onset, we extracted MNs from adult G85R mice that had been injected with mutant SOD1 fibrils, which has been previously reported to induce ALS in these mice [5]. Interestingly, we found that these ALS-resistant MNs were twice as big and had twice as many branches at 40 µm from the soma compared to the un-induced G85R MNs (Fig. 2f-h). Furthermore, ALS-resistant MNs from induced G85R mice were 30-40% longer and more branched compared to NTg controls than end-stage G93A-DL MNs (Fig. 1e-h). This demonstrates that mutant SOD1 expression by itself induces enhanced MN outgrowth and that upon induction and progression of ALS, this phenotype is enhanced in disease resistant MNs. It is also of note than unlike G93A, the G85R mutant loses most of its enzymatic activity [12, 16], further confirming that the enhanced outgrowth seen in mutant SOD1 MNs is not due to altered redox signaling resulting from SOD1 enzymatic activity.

Having established that adult MNs from multiple backgrounds exhibited an enhanced outgrowth independent of ALS onset, we then sought to determine if this phenotype was innate to MNs expressing mutant SOD1 by culturing embryonic MNs. We isolated MNs from individual G93A-DL and NTg pups at E14 and measured outgrowth after 3 days in culture. No significant difference was observed in outgrowth or branching compared to NTg controls (Fig. 2i-k). This data suggests that, the enhanced outgrowth phenotype may be acquired in early in adulthood, rather than exist as an inherent trait of MNs expressing low levels of mutant SOD1. However, given that embryonic MN pools contain both ALS-resistant and ALS-vulnerable motor neurons it could reflect the opposing effects of mutant SOD1 on these different populations of MNs. Alternatively the lack of enhanced outgrowth in embryonic motor neurons might suggest a selective effect on postnatal/adult versus embryonic MNs.

Expression of SOD1G93A in non-transgenic MNs is sufficient to induce increased outgrowth

To determine if SOD1^{G93A} expression in itself could induce enhanced outgrowth in MNs, independently from any potential priming for regeneration that may occur from the surviving MNs responding to ALS onset, we used adeno-associated virus (AAV) to overexpress G93A-YFP, WT-SOD1-YFP and GFP-only in adult MNs isolated from 9-12 month old NTg mice. Viral infections were performed the day the cells were isolated from the spinal cord and expression of the viral vectors was first detectable after 3 days. Because of the delayed expression, we let the cells grow for 10 days in culture. Expressoin of G93A-YFP induced significant outgrowth of MNs compared to WT-SOD1-YFP or GFP-alone. Furthermore, based on fluorescence intensity, we found expression levels of G93A-YFP positively correlated with outgrowth (Fig. 3d). Interestingly, although the population comparisons were not statistically significant (Fig. 3c) , expression of WT-SOD1 was correlated with decreased outgrowth (Fig. 3d), mimicking the trend seen from analyzing outgrowth of MNs isolated from the WT-SOD1 overexpressing transgenic mouse model (Figure 1i-l). In addition to demonstrating that the regenerative capacity of adult motor neurons could be increased by the expression SOD1^{G93A} of independently of ALS or even long-term priming by cell stress, these experiments validated the findings made from comparisons between SOD1 transgenic and non-transgenic mice. The virus experiments also alleviate the concern that we were potentially selecting for different cellular sub-populations when culturing cells from different mouse models or disease states, since in these experiments, the expressed transgene was the only variable. Given that exogenous expression of SOD1^{G93A} enhances regeneration compared to control infected cells strongly argues that this is a cell-intrinsic phenomenon of ALS-resistant motor neurons.

Enhanced outgrowth of ALS-resistant MNs is predominantly cell-intrinsic

There is considerable evidence showing that the SOD1 mutant-mediated ALS disease process is both cell and non-cell autonomous [10, 18, 74, 76]. While synthesis of mutant SOD1 within motor neurons is a primary driver of the disease, expression of mutant SOD1 by other cells such as interneurons, microglia, astrocytes, Schwan cells and T-lymphocytes substantially contribute to the progression of ALS [8-10, 17, 26, 42, 76]. Although our data showing induced outgrowth on adult MNs induced by exogenous overexpression of mutant SOD1 strongly suggests that contaminating non-neural cells do not contribute to this phenotype, our data comparing adult MN cultures from mutant SOD1 and NTg mice might be influenced by non-cell autonomous effects since the cultures contain other cells like microglia and astrocytes. Hence, it is possible that non-neuronal cells were present in different ratios in NTg vs. mutant SOD1 cultures and/or are differentially secreting factors that contribute to the increased outgrowth seen in mutant SOD1 MNs. To test this possibility, we harvested conditioned medium from 3-day-old G93A, G93A-DL, and NTg adult MN cultures and used this medium to culture NTg MNs to see if it could influence neurite out growth. While conditioned media from G93A and G93A-DL MNs did slightly increase outgrowth of NTg MNs, the median difference was only ~5% (Fig. 4 a-c) increase, or roughly 10-20 times less than the median outgrowth differences of G93A, G93A-DL, (Fig. 1a-h), or G85R MNs (Fig. 2g-i) relative to their NTg controls. These data suggest that the observed enhanced outgrowth and branching phenotype of ALS-resistant MNs is not a result of secreted factors from non-neuronal cells, but rather a predominantly intrinsic quality of these MNs. Further, since mutant SOD1 can undergo intercellular transmission [28], it is possible that these

experiments reflect a response to internalized SOD1^{G93A} secreted by the transgenic MNs and not outgrowth factors secreted by non-neuronal cells.

ALS-resistant MNs have increased growth cone size, number, and filopodia length

Previous studies have implicated that SOD1 mutations may be linked to cytoskeletal defects in MNs vulnerable to ALS [47, 75]. Furthermore, G93A has been shown to bind actin and negatively disrupt the actin cytoskeleton [67]. However, enhanced branching and neurite extension are usually associated with actin-based structures, such as the growth cone's lamellipodia and filopodia, which are positive regulators of neurite outgrowth. To investigate whether ALS resistant G93A MNs displayed abnormalities in their actin cytoskeleton, we co-stained end-stage cells for filamentous actin (F-actin) and Tuj-1. Surprisingly, ALS-resistant MNs from G93A and G93A-DL mice had significantly larger growth cones than NTg MNs (Fig. 5). We also found that there was twice as many filopodia per growth cone and the filopodia were 50% longer in ALS-resistant MNs (Fig. 5d, e). Interestingly, this upregulation of actin structures was not present MNs from presymptomatic 2- or 6-month-old mice (Fig. 5f, g), suggesting that as a late-stage adaptation response, MNs upregulate actin-based processes that favor the formation of structures that enhance outgrowth and regeneration.

As mentioned previously, there are several published studies characterizing genetic changes in MNs from G93A mice at various stages of disease progression [19-21, 30, 52, 56, 62, 77]. However, these studies have not reached consensus regarding the underlying genetics promoting ALS resistance, probably due to the variation in experimental design and tissue sampling. For example, using G93A mice, one study found a massive up-regulation of genes involved in cell growth and/or maintenance from micro-dissected motor neurons from the lumbar spinal cord [56], whereas another study found Wnt signaling to be significantly activated when homogenized whole spinal cord was used for RNA extraction [77]. Apart from a single study showing SOD1 binding of actin [67], little is known about actin dynamics in SOD1 driven ALS, although it has been shown that upregulation of axonal guidance genes and actin cytoskeletal genes (including alpha- and beta-actin) occurs from the lumbar spinal cord of pre-symptomatic G93A mouse [20]. This could explain our results showing that well before symptoms become present, G93A MNs are actually primed for outgrowth and regeneration, at least in part due to a positive activation of the actin cytoskeleton. It is also worth noting that Lobsiger *et al.* found that regenerative/injury pathways genes were upregulated both in dismutase active and inactive (G37R and G85R) MNs at disease onset , including ATF3, a gene also known to be upregulated in end stage in G93A mice [11, 41, 59, 70, 71].

In addition, work by Saxena *et al.* demonstrated that gastrocnemius-innervating MNs (presumed to be ALS-vulnerable) have a differential upregulation of endoplamismic reticulum (ER) stress and unfolded protein response (UPR) pathways compared to soleus-innervating MNs (presumed to be ALS-resistant) [63]. Other recent studies have shown that under non-pathological conditions, activation of the UPR can promote axonal regeneration after peripheral nerve injury [54] and that axonal ER-signalling and the UPR upregulate regeneration and the formation of axonal growth cones [53]. Thus, one might speculate that the stronger ER-stress/UPR response of ALS-sensitive MNs to mutant SOD1 overwhelms the MNs and leads to cell death, whereas the more minimal response of ALS-

resistant MNs allows for the pro-regenerative signaling downstream of the UPR to take precedence. While it has been speculated that upregulation of regenerative/injury pathways is merely a compensatory response to mutant SOD1^{G93A}-dependent impairment of axonal regeneration [41, 58] we don't believe this explains the enhanced outgrowth of ALS-resistant MNs since even heterozygote G85R-SOD1:YFP mice, which never develop ALS and therefore do not experience SOD1 mutant dependent MN degeneration, still exhibit the phenotype. Moreover, acute overexpression of mutant SOD1 in cultured adult MNs undergoing regeneration enhances outgrowth, suggesting that a mere compensation response can not soley be responsible for this phenotype. Further studies are needed to determine if the enhanced outgrowth seen in adult ALS resistant MNs is preceded by transcriptional regulation of actin cytoskeletal proteins and if so which stress signals induce this response in early pre-symptomatic stages.

Acknowledgments

This project was supported by a Pathway to Independence Award from the National Institutes of Health (R00 NS087104) to E.A.V.

Figure Legends

Figure 1. G93A and G93A-DL motor neurons from ALS symptomatic mice exhibit an increased outgrowth phenotype. (a) Representative images of motor neurons harvested from symptomatic SOD1-G93A transgenic mice (G93A) and age-matched, non-transgenic (NTg) controls (top) and the same images after tracing and Sholl analysis, color coded to show the number of intersections at various length intervals from the soma (bottom). **(b)** A Sholl graph, representing the average number of neurite branches per distance from the soma, of G93A MNs from symptomatic mice and age-matched NTg controls. **(c)** Box-and-whisker plot of the relative outgrowth (measured as the length of the longest neurite branch) of G93A MNs from symptomatic mice relative to their age-matched NTg controls. **(d)** Box-and-whisker plot of number of intersections present 40 µm (indicated by dotted line in (b) from the soma for G93A MNs from symptomatic mice and NTg controls. For (b), (c), and (d) n=88 from 4 mice and n=120 from 5 mice for NTg and G93A data sets, respectively. **(e)** Representative images (top) and results of Sholl analysis (bottom) of motor neurons harvested from age-matched NTg and symptomatic G93A-DL transgenic mice, demonstrating a pronounced increase in outgrowth and branching of the G93A-DL MNs. **(f)** Sholl graph of G93A-DL MNs from symptomatic mice and age-matched NTg controls. **(g)** Box-and-whisker plot showing the relative increase in outgrowth between NTg controls and G93A-DL MNs from symptomatic mice. **(h)** Box-and-whisker plot showing number of branches 40 µm from the soma for NTg controls and G93A-DL MNs from symptomatic mice. For (f), (g), and (h) n=56 from 3 NTG mice and n=62 from 3 G93A-DL mice. **(i)** Representative images of SOD1^{WT} transgenic mice and their age-matched NTg controls. **(j)** Sholl graph of SOD1^{WT} transgenic mice and their age-matched NTg controls, showing a slight decrease in branching at 40 µm from the soma. **(k)** Box-and-whisker plot of the relative outgrowth between NTg and SOD1^{WT} motor neurons, again a small but significant decrease in outgrowth. **(l)** Box-and-whisker plot showing number of branches 40 µm from the soma for NTg and SOD1^{WT} transgenic MNs. For (j),

(k), and (l) n=82 from 2 mice and n=89 from 3 mice, for NTg and $SOD1^{WT}$, respectively. Error bars on Sholl graphs are 95% confidence intervals. Box-and-whisker plots denote the 95th (top whisker), 75th (top edge of box), 25th (bottom edge of box), and 5th (bottom whisker) percentiles, and the median (bold line in box). Each point on the graph represents an individual cell measurement, scattered with random noise in the x direction to enable visualization of all points for the given data set. p-values were obtained from a two-tailed student's T-test. The image scale bars are 100 µm.

Figure 2. The increased outgrowth phenotype in G93A-DL motor neurons can be observed before onset of ALS symptoms. (a) Representative images of G93A-DL MNs from presymptomatic mice at both 2, 6, and 9 months of age and their age- and gender-matched NTg controls showing a relative increase in outgrowth in G93A-DL MNs presymptomatic mice at 2, 6, and 9 months. **(b)** Line graph representing the fold change in radius between G93A-DL MNs and their age and sex matched NTg counterparts at 2, 6, and 9 months. For (b) and the data set taken at 2 months n=95 for NTg and n=80 for G93A-DL, harvested from 3 mice each. The data set representing 6 months was taken from 3 mice each for NTg and G93A-DL, with n=88 and n=80 respectively. The data set representing 9 months was taken from 3 NTG mice and 3 G93A-DL mice, with n=56 and n=62 respectively. **(c)** Representative images of G93A MNs from 2-month-old presymptomatic mice and their age- and gender-matched NTg controls. **(d)** Sholl graph of G93A MNs from 2-month-old presymptomatic mice and their age-matched NTg controls showing a similar amount of branching and outgrowth between the two. **(e)** Box-and-whisker plot showing relative outgrowth of G93A MNs from 2-month-old presymptomatic mice and their age-matched NTg controls. For (d) and (e) n=60 harvested from 3 mice for NTg and n=60 harvested from 3 mice for G93A. **(f)** Representative images of MNs from heterozygous, 9-month-old G85R transgenic mice, MNs from symptomatic G85R transgenic mice induced to get ALS by injecting spinal cord homogenate from another ALS-symptomatic mouse, and an age- and gender-matched NTg control. **(g)** Sholl graph of MNs from G85R transgenic mice (asymptomatic 9-month-old and symptomatic induced) and their age-matched NTg controls. G85R MNs exhibit increases in outgrowth and branching relative to NTg controls, but this effect is significantly enhanced when the mice are induced to get ALS. **(h)** Box-and-whisker plot showing the relative outgrowth of MNs from G85R transgenic mice (asymptomatic 9-month-old and symptomatic induced) and their age-matched NTg controls. For (g) and (h) n=23 from 2 mice for NTg and n=51 from 4 mice for G85R, n=50 from 2 mice for G85R induced. **(i)** Representative images of E14 NTg and G93A-DL motor neurons, showing the similarity in branching and outgrowth. **(j)** Sholl graph of E14 NTg and G93A-DL motor neurons. **(k)** Box-and-whisker plot depicting relative outgrowth of E14 NTg and G93A-DL motor neurons. For (j) and (k) n=26 and n=17 for NTg and G93A-DL, each harvested from 2 mice. Error bars on Sholl graphs are 95% confidence intervals. Box-and-whisker plots denote the 95th (top whisker), 75th (top edge of box), 25th (bottom edge of box), and 5th (bottom whisker) percentiles, and the median (bold line in box). Each point on the graph represents an individual cell measurement, scattered with random noise in the x direction to enable visualization of all points for the given data set. p-values were obtained from a two-tailed student's T-test (2 conditions) or ANOVA followed by Tukey's post-hoc test (3-4 conditions). The image scale bars are 100 µm.

Figure 3. Exogenous expression of SOD1^{G93A} in non-transgenic adult motor neurons increases outgrowth. (a) Representative images of MNs cultured from NTg mice and infected with either: AAV-GFP, AAV-SOD1-YFP, or AAV-G93A-YFP. Image scale bar is 50 µm**. (b)** Sholl graph showing the decrease in outgrowth demonstrated by MNs overexpressing SOD1. **(c)** Box-and-whisker plot of the neuron radii measured for each cell. For **(b)** and **(c)** n=46, n=45, and n=57, for NTg MNs infected with AAV-GFP, AAV-SOD1-YFP, or AAV-G93A-YFP respectively, cells harvested from 9 mice total, 3 used per experiment. **(d)** Scatterplot demonstrating the relationship between protein expression and overall cell radius in AAV infected NTg MNs. n=38 harvested from 6 mice, n=37 harvested from 6 mice, and n=48 harvested from 6 mice for AAV-GFP, AAV-SOD1-YFP, or AAV-G93A-YFP respectively. For radius analysis, p-values were obtained ANOVA followed by Tukey's post-hoc test. For correlation analysis, r-values were obtained by calculating Pearson correlation coefficient and P-values were calculated assuming a one-tailed distribution.

Figure 4. Culturing non-transgenic motor neurons in media conditioned by G93A or G93A-DL motor neurons does not recapitulate outgrowth phenotype. (a) Representative images of MNs harvested from NTg mice, cultured in medium conditioned (CM) by NTg, G93A, or G93A-DL motor neurons. **(b)** Sholl graph of MNs harvested from NTg mice, cultured in media conditioned by NTg, G93A, or G93A-DL motor neurons, depicting overlapping confidence intervals for all three conditions at all distances from the soma. **(c)** Box-and-whisker plot relative outgrowth of MNs harvested from NTg mice, cultured in medium conditioned by NTg, G93A, or G93A-DL motor neurons, showing a slight but statistically significant increase in outgrowth when NTg MNs are cultured in media conditioned by G93A or G93A-DL cultures. For (b) and (c) n=138 from 4 mice for NTg/NTg-CM, n=134 from 4 mice for NTg/G93A-CM, and n=60 from 2 mice for NTg/G93A-DL-CM. Error bars on Sholl graphs are 95% confidence intervals. Box-and-whisker plots denote the 95th (top whisker), 75th (top edge of box), 25th (bottom edge of box), and 5th (bottom whisker) percentiles, and the median (bold line in box). Each point on the graph represents an individual cell measurement, scattered with random noise in the x direction to enable visualization of all points for the given data set. p-values were obtained ANOVA followed by Tukey's post-hoc test. The image scale bars are 100 µm.

Figure 5. Growth cones and filopodia are larger and more numerous in G93A motor neurons from symptomatic mice. (a) Representative images from motor neurons cultured from NTg, G93A-DL, and G93A mice demonstrating the increase in overall neuron radius, as well as the increase in number of growth cones. Image scale bars are 20 µm **(b)** A magnified look at growth cones from motor neurons cultured from NTg, G93A-DL, and G93A mice, showing the increase in growth cone area, filopodia length, and filopodia per growth cone in G93A and G93A-DL MNs. Image scale bar is 5 µm. **(c)** Box-and-whisker plot depicting growth cone area for MNs cultured from NTg, and G93A-DL mice. **(d)** Box-and-whisker plot depicting the number of filopodia per growth cone for MNs cultured from NTg, and G93A-DL mice. **(e)** Box-and-whisker plot depicting filopodia length for MNs cultured from NTg, and G93A-DL mice. For (c-e) n=25 for NTg, and n=25 for G93A-DL, harvested from two mice for each. **(f)** Line graph representing the fold change in growth cone area between G93A-DL and their NTg controls, normalized to the NTg control for each condition. **(g)** Line graph representing the fold change in filopodia length between NTg and G93A-DL cells, represented as described in (f). For

(f) and (g) 2 NTg and 2 G93A-DL mice were analyzed at each time point. At 2 months n=18 cells for NTg and n=32 cells for G93A-DL. At 6 months n=20 cells for NTg and n=19 cells for G93A-DL. **(h)** Box-and-whisker plot depicting the growth cone area for MNs cultured from NTg and symptomatic G93A mice. **(i)** Box-and-whisker plot depicting filopodia length for MNs cultured from NTg and G93A mice. For (h) and (i) n=38 cells for NTg and n=28 cells for G93A, harvested from 2 mice each. Box-and-whisker plots denote the 95th (top whisker), 75th (top edge of box), 25th (bottom edge of box), and 5th (bottom whisker) percentiles, and the median (bold line in box). Each point on the graph represents an individual cell measurement, scattered with random noise in the x direction to enable visualization of all points for the given data set. p-values were obtained from a two-tailed student's T-test.

References

1 Acevedo-Arozena A, Kalmar B, Essa S, Ricketts T, Joyce P, Kent R, Rowe C, Parker A, Gray A, Hafezparast Met al (2011) A comprehensive assessment of the SOD1G93A low-copy transgenic mouse, which models human amyotrophic lateral sclerosis. Dis Model Mech 4: 686-700 Doi 10.1242/dmm.007237

2 Achilli F, Boyle S, Kieran D, Chia R, Hafezparast M, Martin JE, Schiavo G, Greensmith L, Bickmore W, Fisher EM (2005) The SOD1 transgene in the G93A mouse model of amyotrophic lateral sclerosis lies on distal mouse chromosome 12. Amyotroph Lateral Scler Other Motor Neuron Disord 6: 111-114 Doi 10.1080/14660820510035351

3 Allodi I, Comley L, Nichterwitz S, Nizzardo M, Simone C, Benitez JA, Cao M, Corti S, Hedlund E (2016) Differential neuronal vulnerability identifies IGF-2 as a protective factor in ALS. Sci Rep 6: 25960 Doi 10.1038/srep25960

4 Andersen PM, Al-Chalabi A (2011) Clinical genetics of amyotrophic lateral sclerosis: what do we really know? Nat Rev Neurol 7: 603-615 Doi 10.1038/nrneurol.2011.150

5 Ayers JI, Fromholt SE, O'Neal VM, Diamond JH, Borchelt DR (2016) Prion-like propagation of mutant SOD1 misfolding and motor neuron disease spread along neuroanatomical pathways. Acta Neuropathol 131: 103-114 Doi 10.1007/s00401-015-1514-0

6 Bandyopadhyay U, Cotney J, Nagy M, Oh S, Leng J, Mahajan M, Mane S, Fenton WA, Noonan JP, Horwich AL (2013) RNA-Seq profiling of spinal cord motor neurons from a presymptomatic SOD1 ALS mouse. PLoS One 8: e53575 Doi 10.1371/journal.pone.0053575

7 Beaudet MJ, Yang Q, Cadau S, Blais M, Bellenfant S, Gros-Louis F, Berthod F (2015) High yield extraction of pure spinal motor neurons, astrocytes and microglia from single embryo and adult mouse spinal cord. Sci Rep 5: 16763 Doi 10.1038/srep16763

8 Beers DR, Henkel JS, Xiao Q, Zhao W, Wang J, Yen AA, Siklos L, McKercher SR, Appel SH (2006) Wild-type microglia extend survival in PU.1 knockout mice with familial amyotrophic lateral sclerosis. Proc Natl Acad Sci U S A 103: 16021-16026 Doi 10.1073/pnas.0607423103

9 Beers DR, Henkel JS, Zhao W, Wang J, Appel SH (2008) CD4+ T cells support glial neuroprotection, slow disease progression, and modify glial morphology in an animal model of inherited ALS. Proc Natl Acad Sci U S A 105: 15558-15563 Doi 10.1073/pnas.0807419105

10 Boillée S, Yamanaka K, Lobsiger CS, Copeland NG, Jenkins NA, Kassiotis G, Kollias G, Cleveland DW (2006) Onset and progression in inherited ALS determined by motor neurons and microglia. Science 312: 1389-1392 Doi 10.1126/science.1123511

11 Bonilla IE, Tanabe K, Strittmatter SM (2002) Small proline-rich repeat protein 1A is expressed by axotomized neurons and promotes axonal outgrowth. The Journal of neuroscience : the official journal of the Society for Neuroscience 22: 1303-1315

12 Borchelt DR, Lee MK, Slunt HS, Guarnieri M, Xu ZS, Wong PC, Brown RH, Price DL, Sisodia SS, Cleveland DW (1994) Superoxide dismutase 1 with mutations linked to familial

amyotrophic lateral sclerosis possesses significant activity. Proc Natl Acad Sci U S A 91: 8292-8296

13 Brockington A, Ning K, Heath PR, Wood E, Kirby J, Fusi N, Lawrence N, Wharton SB, Ince PG, Shaw PJ (2013) Unravelling the enigma of selective vulnerability in neurodegeneration: motor neurons resistant to degeneration in ALS show distinct gene expression characteristics and decreased susceptibility to excitotoxicity. Acta Neuropathol 125: 95-109 Doi 10.1007/s00401-012-1058-5

14 Brown RH, Al-Chalabi A (2017) Amyotrophic Lateral Sclerosis. The New England Journal of Medicine: 10

15 Bruijn LI, Becher MW, Lee MK, Anderson KL, Jenkins NA, Copeland NG, Sisodia SS, Rothstein JD, Borchelt DR, Price DLet al (1997) ALS-linked SOD1 mutant G85R mediates damage to astrocytes and promotes rapidly progressive disease with SOD1-containing inclusions. Neuron 18: 327-338

16 Cao X, Antonyuk SV, Seetharaman SV, Whitson LJ, Taylor AB, Holloway SP, Strange RW, Doucette PA, Valentine JS, Tiwari Aet al (2008) Structures of the G85R variant of SOD1 in familial amyotrophic lateral sclerosis. J Biol Chem 283: 16169-16177 Doi 10.1074/jbc.M801522200

17 Chiu IM, Chen A, Zheng Y, Kosaras B, Tsiftsoglou SA, Vartanian TK, Brown RH, Carroll MC (2008) T lymphocytes potentiate endogenous neuroprotective inflammation in a mouse model of ALS. Proc Natl Acad Sci U S A 105: 17913-17918 Doi 10.1073/pnas.0804610105

18 Clement AM, Nguyen MD, Roberts EA, Garcia ML, Boillée S, Rule M, McMahon AP, Doucette W, Siwek D, Ferrante RJet al (2003) Wild-type nonneuronal cells extend survival of SOD1 mutant motor neurons in ALS mice. Science 302: 113-117 Doi 10.1126/science.1086071

19 D'Arrigo A, Colavito D, Peña-Altamira E, Fabris M, Dam M, Contestabile A, Leon A (2010) Transcriptional profiling in the lumbar spinal cord of a mouse model of amyotrophic lateral sclerosis: a role for wild-type superoxide dismutase 1 in sporadic disease? J Mol Neurosci 41: 404-415 Doi 10.1007/s12031-010-9332-2

20 de Oliveira GP, Alves CJ, Chadi G (2013) Early gene expression changes in spinal cord from SOD1(G93A) Amyotrophic Lateral Sclerosis animal model. Front Cell Neurosci 7: 216 Doi 10.3389/fncel.2013.00216

21 Ferraiuolo L, Heath PR, Holden H, Kasher P, Kirby J, Shaw PJ (2007) Microarray analysis of the cellular pathways involved in the adaptation to and progression of motor neuron injury in the SOD1 G93A mouse model of familial ALS. The Journal of neuroscience : the official journal of the Society for Neuroscience 27: 9201-9219 Doi 10.1523/JNEUROSCI.1470-07.2007

22 Ferraiuolo L, Kirby J, Grierson AJ, Sendtner M, Shaw PJ (2011) Molecular pathways of motor neuron injury in amyotrophic lateral sclerosis. Nat Rev Neurol 7: 616-630 Doi 10.1038/nrneurol.2011.152

23 Ferreira TA, Blackman AV, Oyrer J, Jayabal S, Chung AJ, Watt AJ, Sjöström PJ, van Meyel DJ (2014) Neuronal morphometry directly from bitmap images. Nature methods 11: 982-984 Doi 10.1038/nmeth.3125

24 Furukawa Y (2012) Pathological roles of wild-type cu, zn-superoxide dismutase in amyotrophic lateral sclerosis. Neurol Res Int 2012: 323261 Doi 10.1155/2012/323261

25 Gizzi M, DiRocco A, Sivak M, Cohen B (1992) Ocular motor function in motor neuron disease. Neurology 42: 1037-1046

26 Gowing G, Philips T, Van Wijmeersch B, Audet JN, Dewil M, Van Den Bosch L, Billiau AD, Robberecht W, Julien JP (2008) Ablation of proliferating microglia does not affect motor neuron degeneration in amyotrophic lateral sclerosis caused by mutant superoxide dismutase. The Journal of neuroscience : the official journal of the Society for Neuroscience 28: 10234-10244 Doi 10.1523/JNEUROSCI.3494-08.2008

27 Graber DJ, Harris BT (2013) Purification and culture of spinal motor neurons. Cold Spring Harb Protoc 2013: 310-311 Doi 10.1101/pdb.top070920

28 Grad LI, Yerbury JJ, Turner BJ, Guest WC, Pokrishevsky E, O'Neill MA, Yanai A, Silverman JM, Zeineddine R, Corcoran Let al (2014) Intercellular propagated misfolding of wild-type Cu/Zn superoxide dismutase occurs via exosome-dependent and -independent mechanisms. Proc Natl Acad Sci U S A 111: 3620-3625 Doi 10.1073/pnas.1312245111

29 Graffmo KS, Forsberg K, Bergh J, Birve A, Zetterström P, Andersen PM, Marklund SL, Brännström T (2013) Expression of wild-type human superoxide dismutase-1 in mice causes amyotrophic lateral sclerosis. Hum Mol Genet 22: 51-60 Doi 10.1093/hmg/dds399

30 Guipponi M, Li QX, Hyde L, Beissbarth T, Smyth GK, Masters CL, Scott HS (2010) SAGE analysis of genes differentially expressed in presymptomatic TgSOD1G93A transgenic mice identified cellular processes involved in early stage of ALS pathology. J Mol Neurosci 41: 172-182 Doi 10.1007/s12031-009-9317-1

31 Gurney ME (1994) Transgenic-mouse model of amyotrophic lateral sclerosis. N Engl J Med 331: 1721-1722 Doi 10.1056/NEJM199412223312516

32 Haenggeli C, Kato AC (2002) Differential vulnerability of cranial motoneurons in mouse models with motor neuron degeneration. Neurosci Lett 335: 39-43

33 Henriques A, Pitzer C, Schneider A (2010) Characterization of a novel SOD-1(G93A) transgenic mouse line with very decelerated disease development. PLoS One 5: e15445 Doi 10.1371/journal.pone.0015445

34 Ilieva HS, Yamanaka K, Malkmus S, Kakinohana O, Yaksh T, Marsala M, Cleveland DW (2008) Mutant dynein (Loa) triggers proprioceptive axon loss that extends survival only in the SOD1 ALS model with highest motor neuron death. Proc Natl Acad Sci U S A 105: 12599-12604 Doi 10.1073/pnas.0805422105

35 Ince PG, Lowe J, Shaw PJ (1998) Amyotrophic lateral sclerosis: current issues in classification, pathogenesis and molecular pathology. Neuropathol Appl Neurobiol 24: 104-117

36 Jonsson PA, Graffmo KS, Brännström T, Nilsson P, Andersen PM, Marklund SL (2006) Motor neuron disease in mice expressing the wild type-like D90A mutant superoxide dismutase-1. J Neuropathol Exp Neurol 65: 1126-1136 Doi 10.1097/01.jnen.0000248545.36046.3c

37 Kaplan A, Spiller KJ, Towne C, Kanning KC, Choe GT, Geber A, Akay T, Aebischer P, Henderson CE (2014) Neuronal matrix metalloproteinase-9 is a determinant of selective neurodegeneration. Neuron 81: 333-348 Doi 10.1016/j.neuron.2013.12.009

38 Karch CM, Prudencio M, Winkler DD, Hart PJ, Borchelt DR (2009) Role of mutant SOD1 disulfide oxidation and aggregation in the pathogenesis of familial ALS. Proc Natl Acad Sci U S A 106: 7774-7779 Doi 10.1073/pnas.0902505106

39 Kiaei M, Kipiani K, Calingasan NY, Wille E, Chen J, Heissig B, Rafii S, Lorenzl S, Beal MF (2007) Matrix metalloproteinase-9 regulates TNF-alpha and FasL expression in neuronal, glial cells and its absence extends life in a transgenic mouse model of amyotrophic lateral sclerosis. Exp Neurol 205: 74-81 Doi 10.1016/j.expneurol.2007.01.036

40 Lalancette-Hebert M, Sharma A, Lyashchenko AK, Shneider NA (2016) Gamma motor neurons survive and exacerbate alpha motor neuron degeneration in ALS. Proc Natl Acad Sci U S A 113: E8316-E8325 Doi 10.1073/pnas.1605210113

41 Lobsiger CS, Boillée S, Cleveland DW (2007) Toxicity from different SOD1 mutants dysregulates the complement system and the neuronal regenerative response in ALS motor neurons. Proc Natl Acad Sci U S A 104: 7319-7326 Doi 10.1073/pnas.0702230104

42 Lobsiger CS, Boillee S, McAlonis-Downes M, Khan AM, Feltri ML, Yamanaka K, Cleveland DW (2009) Schwann cells expressing dismutase active mutant SOD1 unexpectedly slow disease progression in ALS mice. Proc Natl Acad Sci U S A 106: 4465-4470 Doi 10.1073/pnas.0813339106

43 Longair MH, Baker DA, Armstrong JD (2011) Simple Neurite Tracer: open source software for reconstruction, visualization and analysis of neuronal processes. Bioinformatics 27: 2453-2454 Doi 10.1093/bioinformatics/btr390

44 Lorenzo LE, Barbe A, Portalier P, Fritschy JM, Bras H (2006) Differential expression of GABAA and glycine receptors in ALS-resistant vs. ALS-vulnerable motoneurons: possible implications for selective vulnerability of motoneurons. Eur J Neurosci 23: 3161-3170 Doi 10.1111/j.1460-9568.2006.04863.x

45 Ma L, Ostrovsky H, Miles G, Lipski J, Funk GD, Nicholson LF (2006) Differential expression of group I metabotropic glutamate receptors in human motoneurons at low and high risk of degeneration in amyotrophic lateral sclerosis. Neuroscience 143: 95-104 Doi 10.1016/j.neuroscience.2006.07.058

46 Maher P, Schubert D (2000) Signaling by reactive oxygen species in the nervous system. Cell Mol Life Sci 57: 1287-1305

47 McMurray CT (2000) Neurodegeneration: diseases of the cytoskeleton? Cell Death Differ 7: 861-865 Doi 10.1038/sj.cdd.4400764

48 Morisaki Y, Niikura M, Watanabe M, Onishi K, Tanabe S, Moriwaki Y, Okuda T, Ohara S, Murayama S, Takao Met al (2016) Selective Expression of Osteopontin in ALS-resistant Motor Neurons is a Critical Determinant of Late Phase Neurodegeneration Mediated by Matrix Metalloproteinase-9. Sci Rep 6: 27354 Doi 10.1038/srep27354

49 Munnamalai V, Suter DM (2009) Reactive oxygen species regulate F-actin dynamics in neuronal growth cones and neurite outgrowth. J Neurochem 108: 644-661 Doi 10.1111/j.1471-4159.2008.05787.x

50 Nicholson SJ, Witherden AS, Hafezparast M, Martin JE, Fisher EM (2000) Mice, the motor system, and human motor neuron pathology. Mamm Genome 11: 1041-1052

51 Nimchinsky EA, Young WG, Yeung G, Shah RA, Gordon JW, Bloom FE, Morrison JH, Hof PR (2000) Differential vulnerability of oculomotor, facial, and hypoglossal nuclei in G86R superoxide dismutase transgenic mice. J Comp Neurol 416: 112-125

52 Offen D, Barhum Y, Melamed E, Embacher N, Schindler C, Ransmayr G (2009) Spinal cord mRNA profile in patients with ALS: comparison with transgenic mice expressing the human SOD-1 mutant. J Mol Neurosci 38: 85-93 Doi 10.1007/s12031-007-9004-z

53 Ohtake Y, Matsuhisa K, Kaneko M, Kanemoto S, Asada R, Imaizumi K, Saito A (2018) Axonal Activation of the Unfolded Protein Response Promotes Axonal Regeneration Following Peripheral Nerve Injury. Neuroscience 375: 34-48 Doi 10.1016/j.neuroscience.2018.02.003

54 Onate M, Catenaccio A, Martinez G, Armentano D, Parsons G, Kerr B, Hetz C, Court FA (2016) Activation of the unfolded protein response promotes axonal regeneration after peripheral nerve injury. Sci Rep 6: 21709 Doi 10.1038/srep21709

55 Pasinelli P, Brown RH (2006) Molecular biology of amyotrophic lateral sclerosis: insights from genetics. Nat Rev Neurosci 7: 710-723 Doi 10.1038/nrn1971

56 Perrin FE, Boisset G, Docquier M, Schaad O, Descombes P, Kato AC (2005) No widespread induction of cell death genes occurs in pure motoneurons in an amyotrophic lateral sclerosis mouse model. Hum Mol Genet 14: 3309-3320 Doi 10.1093/hmg/ddi357

57 Piccione EA, Sletten DM, Staff NP, Low PA (2015) Autonomic system and amyotrophic lateral sclerosis. Muscle Nerve 51: 676-679 Doi 10.1002/mus.24457

58 Pun S, Santos AF, Saxena S, Xu L, Caroni P (2006) Selective vulnerability and pruning of phasic motoneuron axons in motoneuron disease alleviated by CNTF. Nat Neurosci 9: 408-419 Doi 10.1038/nn1653

59 Raivich G, Bohatschek M, Da Costa C, Iwata O, Galiano M, Hristova M, Nateri AS, Makwana M, Riera-Sans L, Wolfer DPet al (2004) The AP-1 transcription factor c-Jun is required for efficient axonal regeneration. Neuron 43: 57-67 Doi 10.1016/j.neuron.2004.06.005

60 Rosario AM, Cruz PE, Ceballos-Diaz C, Strickland MR, Siemienski Z, Pardo M, Schob KL, Li A, Aslanidi GV, Srivastava Aet al (2016) Microglia-specific targeting by novel capsid-modified AAV6 vectors. Mol Ther Methods Clin Dev 3: 16026 Doi 10.1038/mtm.2016.26

61 Saccon RA, Bunton-Stasyshyn RK, Fisher EM, Fratta P (2013) Is SOD1 loss of function involved in amyotrophic lateral sclerosis? Brain 136: 2342-2358 Doi 10.1093/brain/awt097

62 Saris CG, Groen EJ, van Vught PW, van Es MA, Blauw HM, Veldink JH, van den Berg LH (2013) Gene expression profile of SOD1-G93A mouse spinal cord, blood and muscle. Amyotrophic lateral sclerosis & frontotemporal degeneration 14: 190-198 Doi 10.3109/21678421.2012.749914

63 Saxena S, Cabuy E, Caroni P (2009) A role for motoneuron subtype-selective ER stress in disease manifestations of FALS mice. Nat Neurosci 12: 627-636 Doi 10.1038/nn.2297

64 Schaefer AM, Sanes JR, Lichtman JW (2005) A compensatory subpopulation of motor neurons in a mouse model of amyotrophic lateral sclerosis. J Comp Neurol 490: 209-219 Doi 10.1002/cne.20620

65 Strang KH, Goodwin MS, Riffe C, Moore BD, Chakrabarty P, Levites Y, Golde TE, Giasson BI (2017) Generation and characterization of new monoclonal antibodies targeting the PHF1 and AT8 epitopes on human tau. Acta Neuropathol Commun 5: 58 Doi 10.1186/s40478-017-0458-0

66 Synofzik M, Fernández-Santiago R, Maetzler W, Schöls L, Andersen PM (2010) The human G93A SOD1 phenotype closely resembles sporadic amyotrophic lateral sclerosis. J Neurol Neurosurg Psychiatry 81: 764-767 Doi 10.1136/jnnp.2009.181719

67 Takamiya R, Takahashi M, Park YS, Tawara Y, Fujiwara N, Miyamoto Y, Gu J, Suzuki K, Taniguchi N (2005) Overexpression of mutated Cu,Zn-SOD in neuroblastoma cells results in cytoskeletal change. Am J Physiol Cell Physiol 288: C253-259 Doi 10.1152/ajpcell.00014.2004

68 Thannickal VJ, Fanburg BL (2000) Reactive oxygen species in cell signaling. Am J Physiol Lung Cell Mol Physiol 279: L1005-1028

69 Tjust AE, Brannstrom T, Pedrosa Domellof F (2012) Unaffected motor endplate occupancy in eye muscles of ALS G93A mouse model. Front Biosci (Schol Ed) 4: 1547-1555

70 Tsujino H, Kondo E, Fukuoka T, Dai Y, Tokunaga A, Miki K, Yonenobu K, Ochi T, Noguchi K (2000) Activating transcription factor 3 (ATF3) induction by axotomy in sensory and motoneurons: A novel neuronal marker of nerve injury. Mol Cell Neurosci 15: 170-182 Doi 10.1006/mcne.1999.0814

71 Vlug AS, Teuling E, Haasdijk ED, French P, Hoogenraad CC, Jaarsma D (2005) ATF3 expression precedes death of spinal motoneurons in amyotrophic lateral sclerosis-SOD1 transgenic mice and correlates with c-Jun phosphorylation, CHOP expression, somato-dendritic ubiquitination and Golgi fragmentation. Eur J Neurosci 22: 1881-1894 Doi 10.1111/j.1460-9568.2005.04389.x

72 Wang J, Farr GW, Zeiss CJ, Rodriguez-Gil DJ, Wilson JH, Furtak K, Rutkowski DT, Kaufman RJ, Ruse CI, Yates JRet al (2009) Progressive aggregation despite chaperone associations of a mutant SOD1-YFP in transgenic mice that develop ALS. Proc Natl Acad Sci U S A 106: 1392-1397 Doi 10.1073/pnas.0813045106

73 Wang J, Slunt H, Gonzales V, Fromholt D, Coonfield M, Copeland NG, Jenkins NA, Borchelt DR (2003) Copper-binding-site-null SOD1 causes ALS in transgenic mice: aggregates of non-native SOD1 delineate a common feature. Hum Mol Genet 12: 2753-2764 Doi 10.1093/hmg/ddg312

74 Wang L, Sharma K, Grisotti G, Roos RP (2009) The effect of mutant SOD1 dismutase activity on non-cell autonomous degeneration in familial amyotrophic lateral sclerosis. Neurobiol Dis 35: 234-240 Doi 10.1016/j.nbd.2009.05.002

75 Williamson TL, Cleveland DW (1999) Slowing of axonal transport is a very early event in the toxicity of ALS-linked SOD1 mutants to motor neurons. Nat Neurosci 2: 50-56 Doi 10.1038/4553

76 Yamanaka K, Boillee S, Roberts EA, Garcia ML, McAlonis-Downes M, Mikse OR, Cleveland DW, Goldstein LS (2008) Mutant SOD1 in cell types other than motor neurons and oligodendrocytes accelerates onset of disease in ALS mice. Proc Natl Acad Sci U S A 105: 7594-7599 Doi 10.1073/pnas.0802556105

77 Yu L, Guan Y, Wu X, Chen Y, Liu Z, Du H, Wang X (2013) Wnt Signaling is altered by spinal cord neuronal dysfunction in amyotrophic lateral sclerosis transgenic mice. Neurochem Res 38: 1904-1913 Doi 10.1007/s11064-013-1096-y

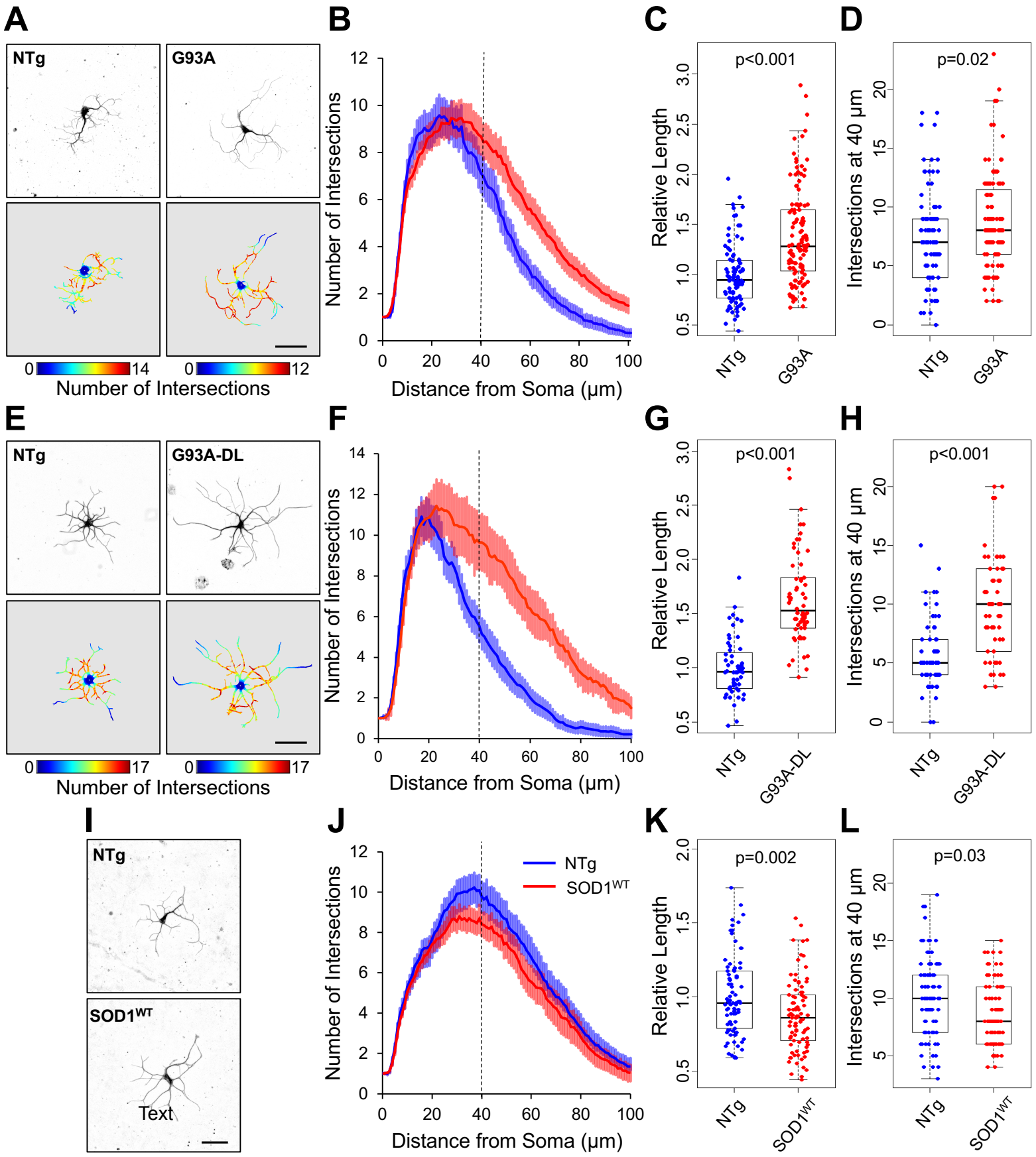
A
NTg
G93A
0
14
0
12
Number of Intersections
B
Number of Intersections
Distance from Soma (µm)
C
p<0.001
Relative Length
NTg
G93A
D
p=0.02
Intersections at 40 µm
NTg
G93A
E
NTg
G93A-DL
0
17
0
17
Number of Intersections
F
Number of Intersections
Distance from Soma (µm)
G
p<0.001
Relative Length
NTg
G93A-DL
H
p<0.001
Intersections at 40 µm
NTg
G93A-DL
I
NTg
SOD1WT
Text
J
NTg
SOD1WT
Number of Intersections
Distance from Soma (µm)
K
p=0.002
Relative Length
NTg
SOD1WT
L
p=0.03
Intersections at 40 µm
NTg
SOD1WT

Figure 1

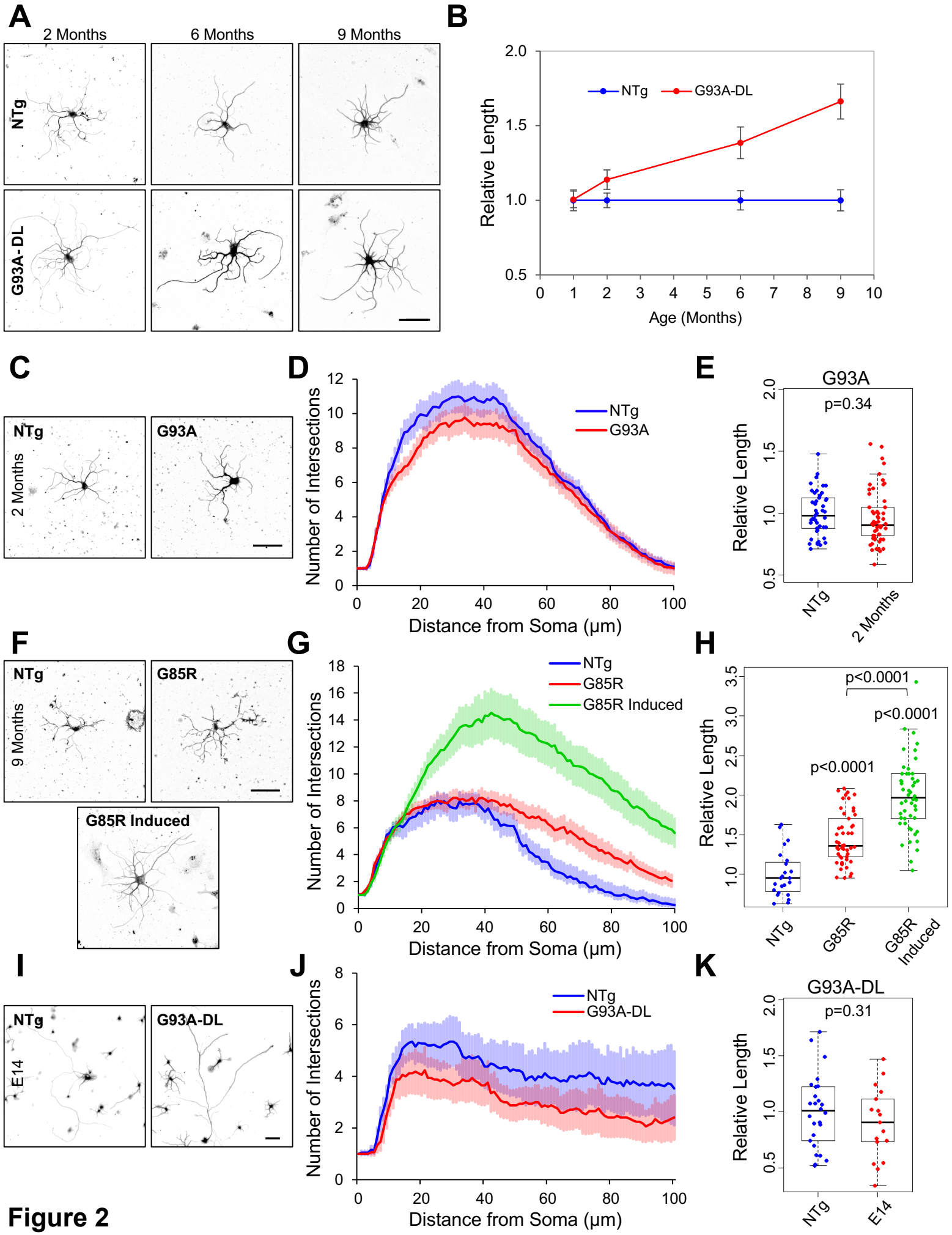
A
2 Months
6 Months
9 Months
NTg
G93A-DL
B
NTg
G93A-DL
Relative Length
Age (Months)
C
NTg
G93A
2 Months
D
NTg
G93A
Number of Intersections
Distance from Soma (µm)
E
G93A
p=0.34
Relative Length
NTg
2 Months
F
NTg
G85R
9 Months
G85R Induced
G
NTg
G85R
G85R Induced
Number of Intersections
Distance from Soma (µm)
H
p<0.0001
p<0.0001
p<0.0001
Relative Length
NTg
G85R
G85R Induced
I
NTg
G93A-DL
E14
J
NTg
G93A-DL
Number of Intersections
Distance from Soma (µm)
K
G93A-DL
p=0.31
Relative Length
NTg
E14

Figure 2

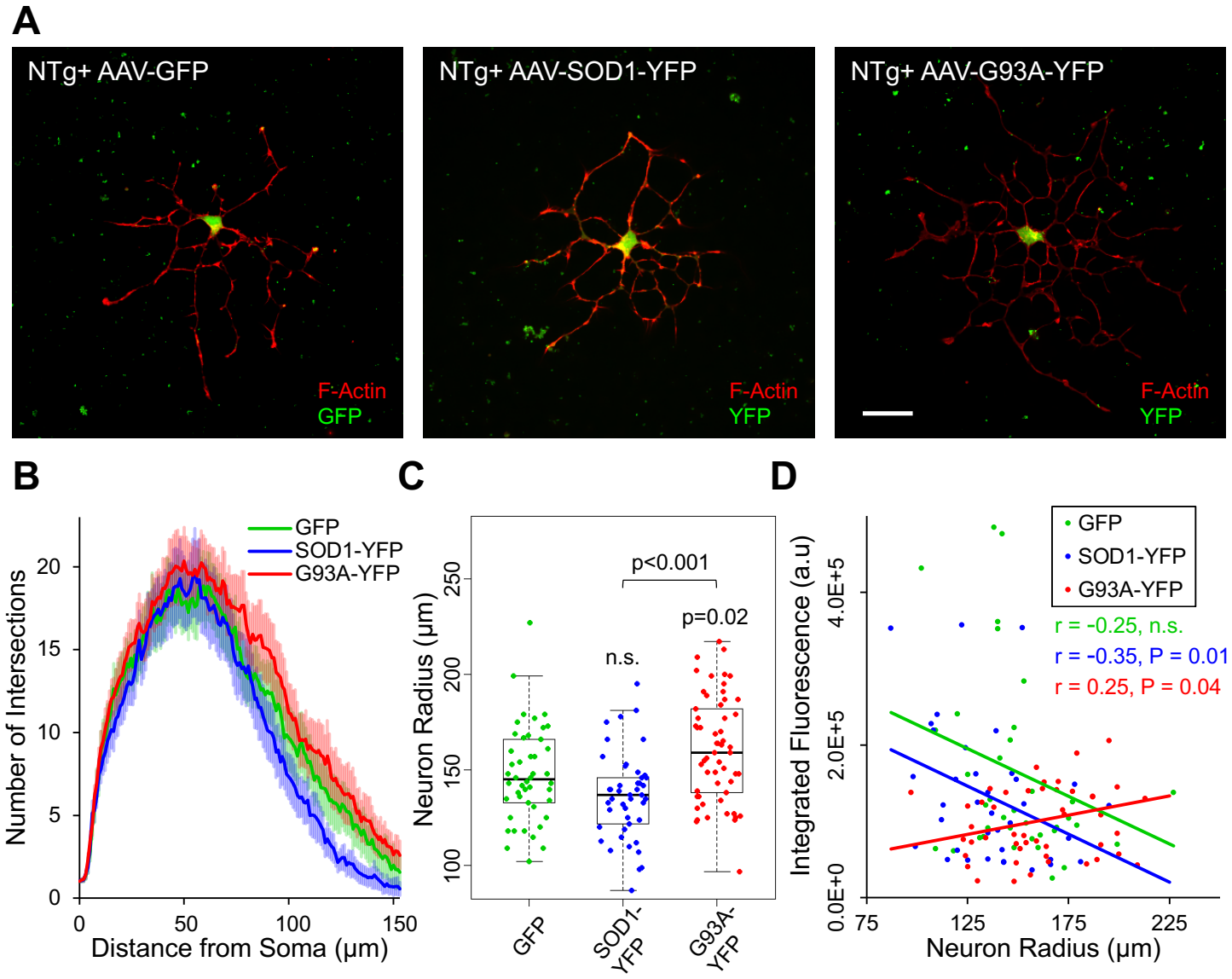
A
NTg+ AAV-GFP
F-Actin
GFP
NTg+ AAV-SOD1-YFP
F-Actin
YFP
NTg+ AAV-G93A-YFP
F-Actin
YFP
B
GFP
SOD1-YFP
G93A-YFP
Number of Intersections
Distance from Soma (µm)
C
p<0.001
p=0.02
n.s.
Neuron Radius (µm)
GFP
SOD1-YFP
G93A-YFP
D
GFP
SOD1-YFP
G93A-YFP
r = -0.25, n.s.
r = -0.35, P = 0.01
r = 0.25, P = 0.04
Integrated Fluorescence (a.u)
Neuron Radius (µm)

Figure 3

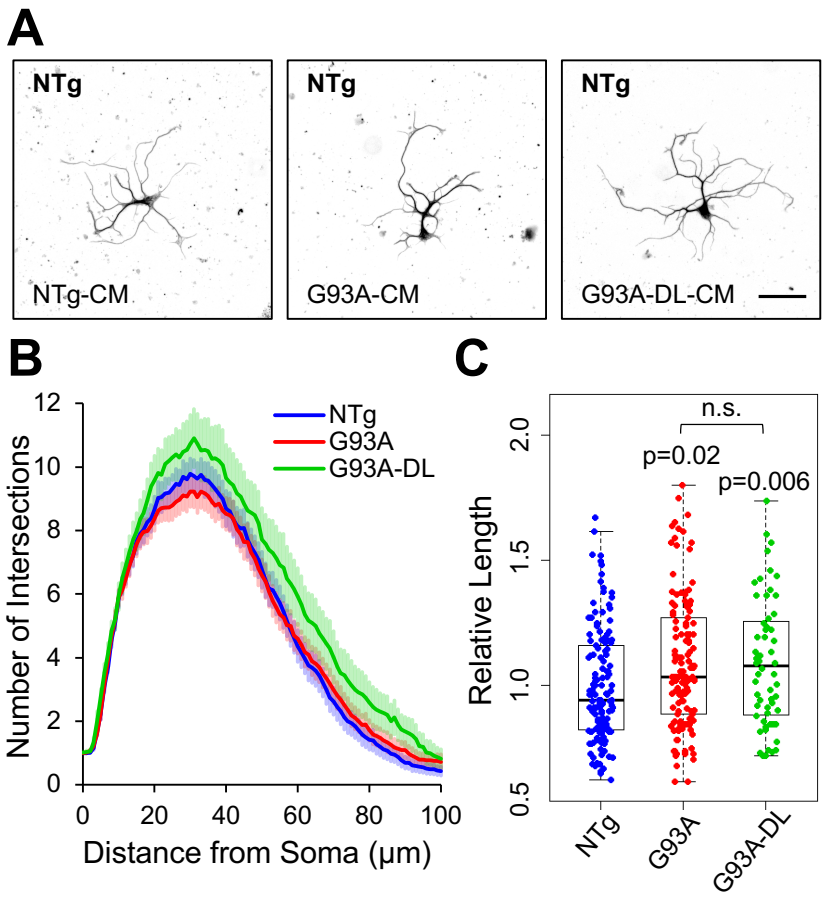
A
NTg
NTg-CM
NTg
G93A-CM
NTg
G93A-DL-CM
B
Number of Intersections
Distance from Soma (μm)
NTg
G93A
G93A-DL
C
Relative Length
n.s.
p=0.02
p=0.006
NTg
G93A
G93A-DL

Figure 4

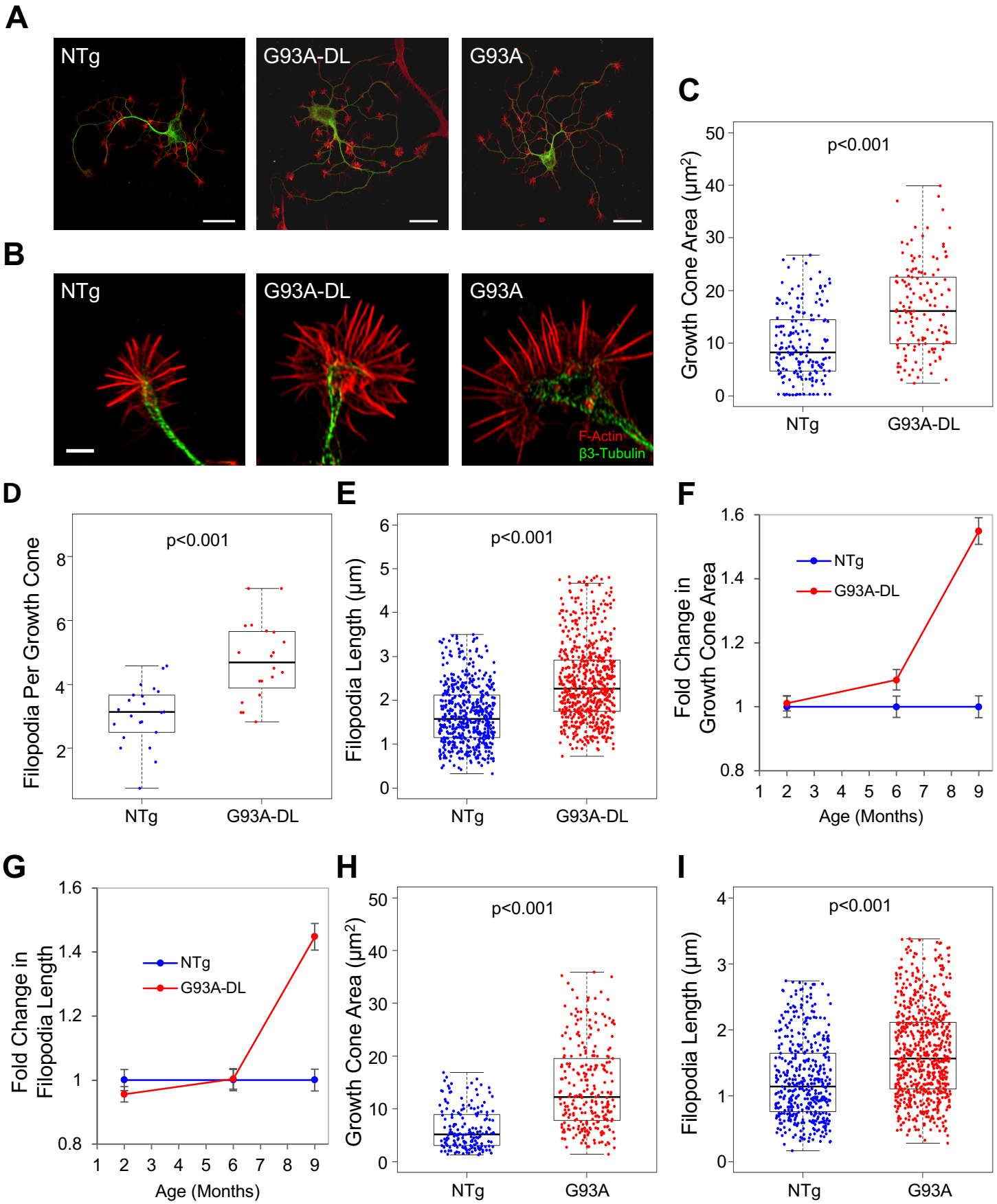
A
NTg
G93A-DL
G93A
B
NTg
G93A-DL
G93A
F-Actin
β3-Tubulin
C
p<0.001
Growth Cone Area (μm²)
NTg
G93A-DL
D
p<0.001
Filopodia Per Growth Cone
NTg
G93A-DL
E
p<0.001
Filopodia Length (μm)
NTg
G93A-DL
F
NTg
G93A-DL
Fold Change in Growth Cone Area
Age (Months)
G
NTg
G93A-DL
Fold Change in Filopodia Length
Age (Months)
H
p<0.001
Growth Cone Area (μm²)
NTg
G93A
I
p<0.001
Filopodia Length (μm)
NTg
G93A

Figure 5